Preprint version of:
Sanchez-Laulhe E, Ruiz C, Acosta J Á and Ollero A (2022), Fuselage Aerodynamics and Weight Trad-Off at Low-Speed Ornithopter Flight,
In 2022 International Conference of Unmanned Aircraft Systems (ICUAS), June 2022, pp. 310-318.

# Fuselage Aerodynamics and Weight Trade-Off at Low-Speed Ornithopter Flight

E. Sanchez-Laulhe*[1], C. Ruiz[2], J.Á. Acosta[2], A. Ollero[2]

***Abstract*— This work presents a thorough study on the effect of the inclusion or not of a fuselage in flapping wing robots, for which no clear criterion has been found so far. The study consists of a dynamic analysis for level flight conditions at both configurations of an actual prototype. An overall aerodynamic model based on CFD simulations is used for modeling the average in-flight forces performed by the ornithopter elements, wing, body, and tail. Experimental thrust correction is developed to include the effects of wing flexibility, thus increasing the accuracy of the results. Results show better performance at low speeds when the ornithopter does not carry the fuselage. At higher speeds, the lower drag provided by the fuselage becomes important. However, the increased weight always needs a higher flapping frequency for the low velocity range of our prototype, creating a disadvantage for this regime. The results highlight a fuselage design criteria, which can be extrapolated to other bird-scaled flapping wing robots performing slow maneuvers, such as perching, as well as to hybrid flapping-fixed wing UAVs.**

## I. Introduction

Aerial platforms with the capability of moving their wings resembling the behavior of birds are particularly interesting for real-world applications in close proximity to humans and structures. This makes these bio-inspired Unmanned Aerial Vehicles(UAVs) particularly interesting in situations where physical interaction is needed, and they are increasingly becoming a feasible alternative to those traditionally based on fast-rotating propellers. Altogether make them a promising technology to perform safe and reliable aerial flights.

In this work, we focus on the aerodynamics of such UAVs which are able to physically interact with their environment, possibly with humans. Even though physical interaction is a common task for birds, the ability of aerial robots to resemble it is still quite limited. The main difficulty is being able to fly and control low-speed maneuvers which rely on high amplitude flapping to generate enough thrust.

There are several projects focused on research and development of ornithopters. Small scale prototypes, such as the Robobee [1] or the BatBot [2], resemble the behavior of insects or small birds, with complex wing kinematics that provide high maneuverability, including also the ability of performing hovering operations.

This work has been partially supported by the European Union H2020 GRIFFIN ERC Advanced Grant 2017, Action 788247, the AERIAL-CORE, Contract 871479 and by PAIDI 2020 HOMPOT project PY20_00597. ESL also acknowledges his predoctoral contract at the Universidad de Málaga

*Corresponding author

[1]University of Malaga, Mecanica de Fluidos, Dr Ortiz Ramos S/N, 29071, Malaga, Spain. ernesto.slaulhe@uma.es

[2]Universidad de Sevilla, GRVC Robotics Lab., Camino de los Descubrimientos S/N 41092, Seville, Spain. crpaez@us.es, jaar@us.es, aollero@us.es

Regarding bird-scale ornithopters, existing prototypes go from medium to large scale. For instance, the Dove [3] and ThunderI [4] are in the range of 200-350 g and a wingspan around 0.5 m, flying at speeds around 10 m/s. Meanwhile, the RoboRaven project [5] provides a larger solution (200-700 g), with low operational speeds around 6 m/s. On the other hand, Robird Falcon (730 g) and Bald Eagle (2.1 kg) [6] are the faster existing prototypes with operational speeds of 16 m/s and 18 m/s respectively.

However, in all of the aforementioned prototypes the lack of payload capabilities and computational power limit their perception subsystems and then makes it more difficult to perform autonomously safe physical interaction tasks.

Fig. 1. GRIFFIN ornithopter prototype with fuselage and camera case in the head.

For large flapping-wing aerial robots, those common birds tasks become a challenge, which is the case of study in this work. Thus, in the context of the GRIFFIN Advanced Grant of the European Research Council, we have developed a fully operational large aerial robot with available payload and low-speed operational range (2-6 m/s) [7], with characterized aerodynamics [8], [9], to perform real-world applications based on the perception of the environment. As a new addition to this prototype, a fuselage body has been designed in order to get a bird appearance, providing also impact resistance and better aerodynamic performance in forward flight. We see the prototype with the new fuselage in Fig. 1, However, in those applications, the full perception system is

mounted onboard and then the available payload becomes quite limited. Therefore, in this task-oriented application the fuselage adds extra weight and possibly reduces the low-speed maneuverability. Of course, in a platform with more payload, this would not be a problem, but the current technology does not allow that without enlarging the 1.5 m wingspan, which would go against the ultimate goal of flying safely in proximity to humans. As usual in engineering, we find contradictory requirements that make us take trade-off solutions eventually.

The aerodynamics studies in the above mentioned prototypes are concerned mainly in the flapping wing or in the tail. However, there is no analysis of the influence of the body and the advantages of an aerodynamic design of a fuselage body, especially when the aforementioned task is a requirement. Airplanes normally design their fuselage in order to reduce the aerodynamic drag, improving energy efficiency. This structure is needed in order to protect the payload at the high speeds and altitudes aircraft fly. However, ornithopters fly considerably slower and at low heights. Therefore, the fuselage body is not always a necessity to operate. In fact, it adds more weight, which is a problem given the limited payload that these UAVs usually have. For that reason, we observe different choices for the design of the body in existing ornithopters. For instance, ThunderI adds just a frontal protection over the skeleton, that works as a frontal fuselage. RoboRaven does not use any protective structure, having its mechanism directly frontal to the airflow. Meanwhile, faster ornithopters, such as the Dove and Robird prototypes, have developed a complete fuselage body around the mechanism as a protection from the airflow and impacts, improving the aerodynamic performance.

The disparity of choices in those prototypes makes us wonder if the addition of a fuselage body provides an actual operational advantage or not. Furthermore, the fact that faster existing prototypes choose to use it, while the slow ones prefer not to carry the additional load, leads to a possible answer. In this work, and to the best of the author's knowledge for the first time, we provide the answer that the advantages of the fuselage in ornithopters depend on the operational conditions of the task for which they were made.

The contribution of this article consists of an operational study of an ornithopter flight which leads to the decision about carrying a fuselage. Two cases are analyzed with and without fuselage. Dynamic analysis is based on aircraft flight equations, using results of CFD experimentally validated [8], [9] for the formulation of the aerodynamic forces. In order to model the aerodynamic performance of the fuselage, a new CFD analysis is also developed. Thrust formulation is corrected to take into account the contribution of wing flexibility. Considering conditions of level flight, an operational comparison is presented. The results are limited to the longitudinal plane as just symmetrical behavior is considered.

The results of this paper can be applied to both flapping wing and hybrid flapping/fixed wing UAVs as considered in the AERIAL-CORE H2020 project[10].

The paper is structured as follows. Section II provides information about the design and optimization of the fuselage. Then, section III develops the flight dynamic equations. The aerodynamic forces are modeled in section IV, with the correction of the thrust explained in section IV-C.2. Finally, simulation results are presented in section V.

## II. Fuselage Design

The design and manufacturing of the Griffin fuselage have been carried out by FADA-CATEC [11]. The optimized geometry was obtained based on stress analysis in Ansys. The main requirements for the optimization of the structure were the manufacturing material Polyamide 12 and the lightweight. The final design is shown in Fig. 2.

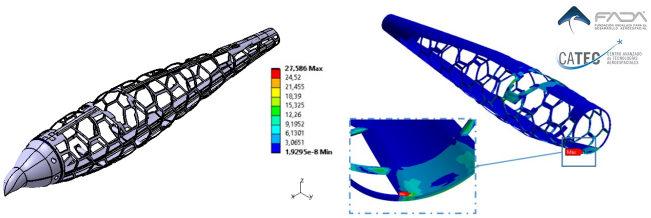


Fig. 2. Fuselage design CAD (left) and stress analysis (right). Courtesy of FADA-CATEC [11]

The load and boundary conditions have been estimated based on the stress to which the structure will be subjected as: embedding in the junction of the fuselage and head, moments generated by the flapping wings and a force at the bottom emulating the impact when landing on the ground. The results based on Von Mises stress and displacements are shown in Fig. 2.

Finally, the fuselage was built with the additive manufacturing technology named Selective Laser Sintering, in which polymer powder particles of Polyamide 12 are sintered to fuse them locally. Other designs manufactured by FADA-CATEC with these technologies are in [12], [13], [14].

The optimized fuselage adds a weight of 82 g as shown in Fig. 2 and 93 g with the covering fabric as shown in Fig. 1. The studies developed in this article consider this increase, compared to the prototype presented in [7]. However, it should also provide a better aerodynamic performance, eliminating the protective frontal body used in that work.

## III. Dynamic Analysis

The analysis developed in this section consists of a comparison between the behavior of the ornithopter with the fuselage and without it in level flight conditions. Parameters used and their nomenclature are defined in Table I. Fig. 3 shows how those variables are defined in the ornithopter.

Level flight conditions consist of a steady state with symmetrical behavior, so dynamics outside the longitudinal plan are not considered. In addition, the velocity vector of the prototype is in the horizontal plane. With those conditions,

TABLE I

NOMENCLATURE

| Variable | Parameter |
|---|---|
| $W(N)$ | Weight of the ornithopter |
| $L(N)*$ | Global aerodynamic lift |
| $D(N)*$ | Global aerodynamic drag |
| $T(N)$ | Thrust |
| $C_L*$ | Global lift coefficient of the ornithopter |
| $C_D*$ | Global drag coefficient of the ornithopter |
| $\rho(kg/m^3)$ | Air density |
| $U(m/s)$ | Flight velocity |
| $S(m^2)$ | Wing surface |
| $S_t(m^2)$ | Tail surface |
| $\Lambda$ | Surface relation $(S_t/S)$ |
| $c(m)$ | Mean chord |
| $\alpha(^\circ)$ | Angle of attack |
| $k$ | Reduced frequency |
| $f(Hz)$ | Frequency of flapping motion |
| $l_w$ | Distance from wing aerodynamic center to the center of gravity |
| $l_t$ | Distance from tail aerodynamic center to the center of gravity |
| $\delta_e(^\circ)$ | Deflection of the tail |
| $*$ | Found with the subscripts w, b and t they refer to the wing, body and tail respectively. |

the equations that rule the flight are given by

$$W = L = \frac{1}{2}\rho U^2 S C_L \tag{1}$$

$$T = D = \frac{1}{2}\rho U^2 S C_D \tag{2}$$

The fuselage affects mainly by two parameters, the weight, and the drag coefficient. It also has a small contribution over the lift coefficient, almost negligible when compared with the entire lift. Therefore, from equation (1), we can obtain the velocity needed for flight for the same lift as a function of the weight,

$$U = \sqrt{\frac{2W}{\rho S C_L}} \tag{3}$$

being useful to study the effect of the weight on the flight velocity. Alternatively, we can analyze the lift coefficient needed to fly at a certain velocity,

$$C_L = \frac{2W}{\rho U^2 S} \tag{4}$$

For both the lift and drag coefficients, there are three contributions, namely the wing, the tail, and the body. Those aerodynamic contributions are modeled separately in §IV. The global coefficients are defined as

$$C_L = C_{L,w} + C_{L,b} + \Lambda C_{L,t} \tag{5}$$

$$C_D = C_{D,b} + \Lambda C_{D,t} \tag{6}$$

and the contributions can be expressed as a function of the angle of attack and the reduced frequency. Tail coefficient also includes the deflection of the tail. In the case of the ornithopter, the thrust needed to overcome the drag is produced by the wing. Hence, the contribution of the wing to the drag is included in the thrust formulation. The reduced frequency is given by

$$k = \frac{\pi f c}{U}, \tag{7}$$

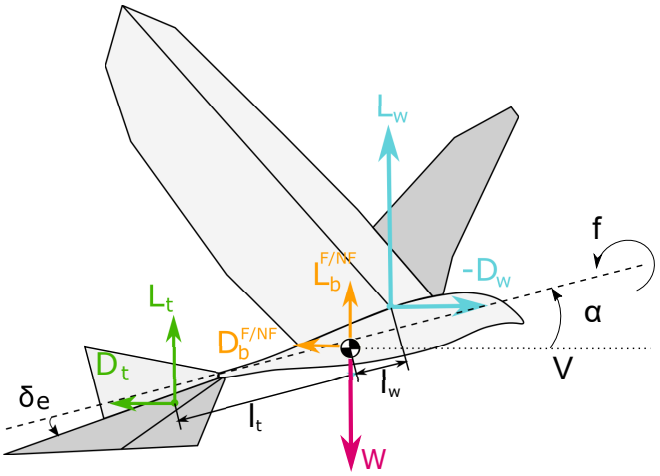


Fig. 3. Forces produced by the different elements of the ornithopter.

It is important to consider also the equilibrium of momentum in the ornithopter, given by the moments generated by the lift forces of both the wing and the tail,

$$0 = L_w l_w + L_t l_t = \frac{1}{2}\rho U^2 S\left(C_{L,w} l_w + \Lambda C_{L,t} l_t\right) \tag{8}$$

The needed thrust is obtained by equation (2), through the drag coefficient defined by the tail and the body. It can be expressed as a function only of the weight and the aerodynamic coefficients

$$T = W\frac{C_D}{C_L} \tag{9}$$

With equations (3)-(9), a direct relation between the control variables, namely the deflection of the tail and the flapping frequency, is defined in order to obtain the conditions for level flight. However, it is more interesting to define the conditions by the frequency needed to fly at a certain velocity or a certain angle of attack. Then, we can obtain the deflection of the tail needed by equation (8). To complete the formulation done here, we need the aerodynamic coefficients formulated in section IV.

## IV. AERODYNAMIC MODELING

In order to obtain the aerodynamic model of the complete ornithopter for the dynamic analysis, separate aerodynamics models of the ornithopter body (with and without fuselage), wings and tail have been made. While a single degree of freedom is taken into account for the body simulation, that is the angle of attack, the influences of the reduced frequency on the wing and the control deflection on the tail have been included, which are presented in the following sections. The models are primarily based on Computer Fluid Dynamics (CFD) numerical simulations and identification method. In addition, the empirical correction of the wing thrust model due to the elasticity of the wing is also included.

### A. Fuselage modeling

A set of CFD simulations of the body with and without the fuselage has been carried out for the present study. The

Reynolds-Average Navier-Stokes (RANS) model is chosen, in particular the $k-\omega$ with Low Reynolds correction, an incompressible two equation Eddy-viscosity model commonly used in intermediate-range Reynolds aerodynamics, and a pressure-velocity coupled scheme, with a first order implicit time discretization for the transient simulation. The fuselage has been modeled as a continuum body with no holes, while the non-fuselaged body geometry has been simplified to improve simulation performance. The geometry can be found in figures 4 and 5.

The fluid has been meshed by tetrahedrons, of the order of

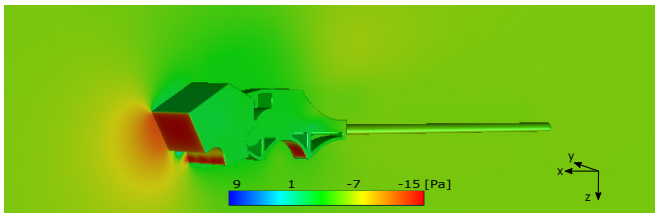


Fig. 4. Pressure contours at angle of attack 20deg and $V = 4m/s$ around the ornithopter's body without fuselage.

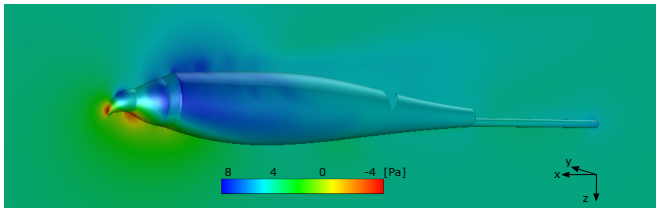


Fig. 5. Pressure contours at angle of attack 20deg and $V = 4m/s$ around the ornithopter's body with fuselage. Note that the colorbar is scaled at each simulation, so they are not comparable between figures.

3M elements approximately, refined near the bodies at the length of $1mm$. Mesh sensitivity analysis has been carried out with no noticeable differences. Several steady simulations have been performed at low velocities (U= 4 m/s) in the range of angle of attack of interest $\alpha = [-30, 30]$ deg. The longitudinal forces and moments produced by the body in both cases are projected in the aerodynamic reference frame, providing lift and drag forces $L_b^{F/NF}$,$D_b^{F/NF}$, of the fuselage (F) and no-fuselage (NF) configurations. The aerodynamic coefficients are constructed as follows

$$C_{L,b}^{F/NF} = \frac{L_b^{F/NF}}{\frac{1}{2}\rho U^2 S} \tag{10}$$

$$C_{D,b}^{F/NF} = \frac{D_b^{F/NF}}{\frac{1}{2}\rho U^2 S} \tag{11}$$

The results obtained are shown in Figure 6. The single points represent the CFD solutions, which have been used to identify through regression a polynomial model to better analyze their contribution to the ornithopter dynamics. The model is given by

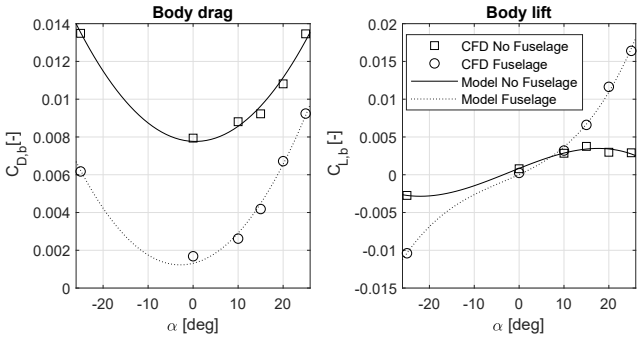


Fig. 6. Lift and drag coefficients of the body, without and with fuselage, obtained at different angle of attack from CFD calculations (squares and circles respectively). Continuous lines represents the identified model.

$$C_{D,b}^{F/NF} = \Theta_D^{F/NF} \begin{bmatrix} 1 \\ \alpha \\ \alpha^2 \end{bmatrix} \tag{12}$$

$$C_{L,b}^{F/NF} = \Theta_L^{F/NF} \begin{bmatrix} 1 \\ \alpha \\ \alpha^2 \\ \alpha^3 \end{bmatrix} \tag{13}$$

Note that while $C_{D,b}^{F/NF}$ is a par function, the quadratic term is included, while on the contrary, for $C_{L,b}^{F/NF}$ identification, it is necessary to include the cubic term. Finally, a regression factor greater than 99 percent has been reached for those parameters presented in Table II, whose results are shown as continuous lines in Figure 6.

TABLE II

IDENTIFIED COEFFICIENTS OF THE BODY'S FORCES MODELS.

| | | | | |
|---|---|---|---|---|
| $\Theta_D^F$ | 0.0013 | 0.0033 | 0.0334 | - |
| $\Theta_D^{NF}$ | 0.0077 | -0.0005 | 0.0291 | - |
| $\Theta_L^F$ | 2.17 e-5 | 0.0156 | 0.0165 | 0.0809 |
| $\Theta_L^{NF}$ | 8.39 e-4 | 0.0135 | -0.0043 | -0.0381 |

## B. Tail modeling

The tail must produce sufficient forces to balance the moments produced by the rest of the elements in the center of gravity when performing a balanced flight, so it is crucial to define the flight envelope and dynamic analysis of the whole ornithopter. For this analysis, an inverted T-tail (see figure 1) has been used. The longitudinal forces are controlled by the deflection of the horizontal plane, $\delta_e$. The aerodynamic model of the tail at different velocities, angles of attack, and elevator deflection is used for the dynamic analysis, which is based on the CFD simulations and identified by a "delta wing" type model, including the stall effect. The model is valid in the range of $\delta_e, \alpha = [-30, 30]$ deg. A representation of the pressure contour and streamlines over the tail is presented in Figure 7.

Analogous to body forces in Equations 12 and 13, the tail model shown in Equations 14 and 15, has been non-

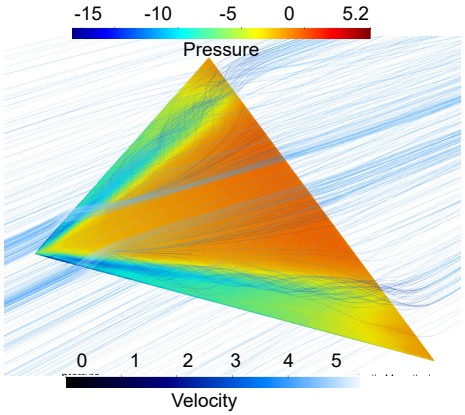


Fig. 7. Contour plot of pressure and streamlines over the tail, at $U = 4m/s$ and $\delta_e = 20\,\text{deg}$ [8]

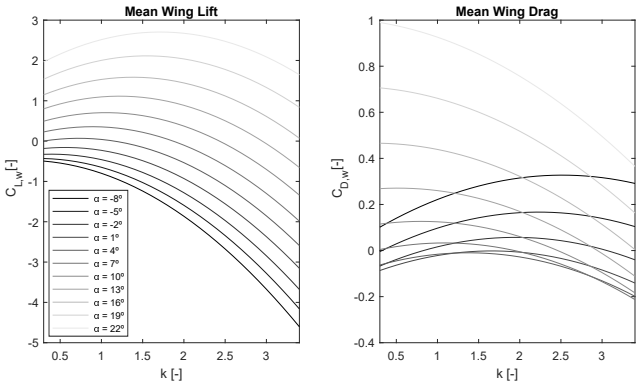


Fig. 8. Lift and drag coefficients of the wing from [9]. Note that as the wing is rigid, the thrust coefficient ($-C_D$) remains small, so the elastic correction will improve the results (see Section IV-C.2).

dimensionalized by the tail surface, being corrected in equations (5)-(6).

$$C_{L,t} = C_{L,t}^{max} \sin\left(a_\alpha(\delta_e + \alpha)\right) \tag{14}$$

$$C_{D,t} = C_{D,t}^{max} - \left(C_{D,t}^{max} - C_{D,t}^{0}\right) \cos\left(b_\alpha(\delta_e + \alpha)\right) \tag{15}$$

The coefficients have been identified with a regression factor greater than 97 percent, and are as follows: $C_{L,t}^{max} = 0.94$, $a_\alpha = 2.92$, $C_{d,t}^{max} = 0.36$, $C_{d,t}^{0} = 0.04$ and $b_\alpha = 4.23$. For further information about the design, aerodynamic simulations and performance analysis and maneuverability we refer to [8], where three different tails at the range of interest were modeled and analyzed experimentally.

### C. Wing modeling

The modeling of the forces exerted by an elastic flapping wing is complex because it involves the simultaneous solution of the non-stationary three-dimensional fluid field and the structure of the elastic wing. While the effect of elasticity on the lift can be neglected, it plays a major role on the thrust. Therefore, for the modeling of the aerodynamic forces on the wing, an accurate CFD model of a rigid flapping wing has been used, and the thrust model has been experimentally corrected as shown below.

*1) Rigid wing modeling:* The wing aerodynamics of the E-flap flapping wing is an unsteady three-dimensional phenomenon, accurately modeled in previous studies [9]. However, for flight dynamics analysis, only the mean values of the forces developed by the wings are needed, which are characterized by the flapping frequency. For that purpose, the model presented in [9] is used, and the mean values are extracted as a function of the reduced frequency and angle of attack, as shown in Figure 8.

*2) Experimental elastic correction of the thrust:* The thrust given by flapping rigid wing is limited when compared with a flexible wing. For this reason, CFD results from [9] give an underestimated thrust coefficient compared with the real one observed in experiments [7]. To estimate the additional thrust given by chordwise flexibility, we use results from theoretical aerodynamic work [15] which study the aerodynamic forces generated by a flapping oscillating airfoil with a quadratic deflection.

The quadratic deflection along the chord comes defined by a quadratic deflection ($\delta_m$) and a pivoting point $p$. The deflection is measured from experimental data. For that goal, we measure the deflection of the trailing edge. In order to convert the measured deflection we have to consider the position of the pivoting point and the dimensions, obtaining

$$\delta_m(f) = \frac{1}{(1-p)^2} \frac{2\Delta z_e(f)}{c} \tag{16}$$

The thrust of an elastic wing can be obtained by correcting the rigid wing model by a given factor to estimate the wing deflection. For this purpose, bench flapping wing experiments have been performed at different frequencies. Several passive markers have been positioned along the chord and span of the wing, as in Figure 9. In this way, a Motion Capture System measures the three-dimensional position of each marker over time, with a frequency of 120 Hz and a precision of the order of $1mm$.

By postprocessing the data, the section $j$ deflection $\theta_e^i$ in degrees and the trailing edge deflection $\Delta z_e^j$ is obtained for each wing section by subtracting the theoretical rigid displacement which is known a priori, which is presented in Figure 10. Note that a quadratic dependence with the

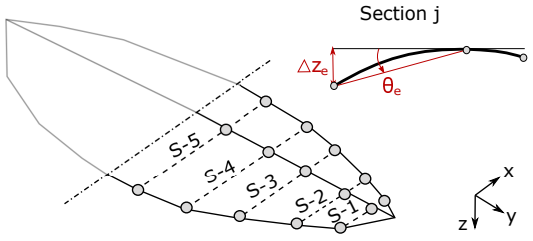


Fig. 9. Positioning of the markers through the half wing.

frequency can be found. The outer section of the wing has less deformation due to the shorter chord, with the exception of the last section, which presents a slightly lower deformation than its neighbor, due to the boundary condition

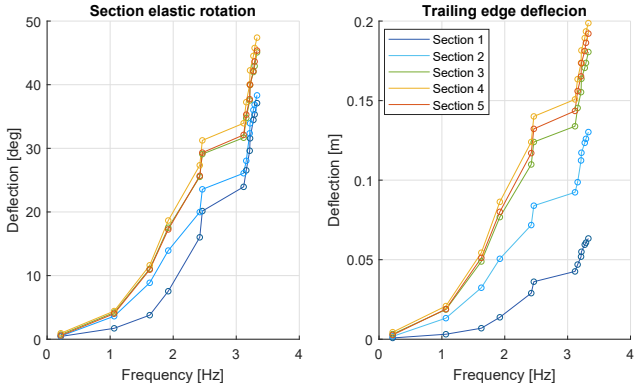


Fig. 10. Deflection of the wing measured at different sections and flapping frequencies. The figure shows the chord deformation of the section $\theta_e^j(f)$ and the deflection of the trailing edge of the section $\Delta z_e^j(f)$. For clarification, see Figure 10.

in the socket, whose trailing edge is not free.
The mean deflection of the trailing edge of the wing can be constructed as a function of the flapping frequency $f$ as follows:

$$\Delta z_e(f) = \sum_{j=1}^{n} \frac{(1-\frac{p}{2})c^j \sin\theta_e^j(f))}{n} \tag{17}$$

Where the number of sections measured is $n = 5$, and $c^j$ is the chord of section $j$. In this case, the pivoting point is defined, by the construction of the wing, at a quarter chord measured from the leading edge ($p = -0.5$). Then, by using (16), the normalized deflection used to correct the thrust is obtained and presented in Figure 11.

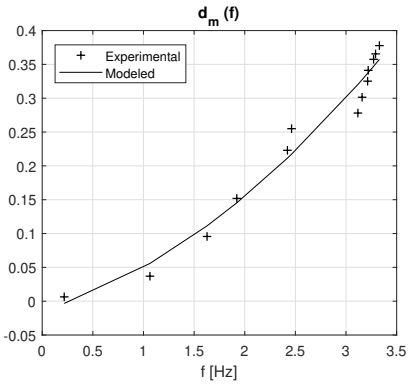


Fig. 11. Experimental normalized deflection used for thrust elastic correction in function of the frequency.

Finally, a non-dimensional deflection model (18) is identified from the experimental data shown in Figure 11, whose parameters with a 98 percent regression quality are: $\Theta_{\delta_m} = [-1.37\ 4.37\ 2.03]\ 10^{-2}$.

$$\delta_m = \Theta_{\delta_m} \begin{bmatrix} 1 \\ f \\ f^2 \end{bmatrix} \tag{18}$$

## V. Results

With the coefficients defined in §IV and §IV-C.2, the dynamic analysis proposed in §III can be developed numerically. In this case, given that both lift and thrust depend on the angle of attack and the reduced frequency, the system has to be solved entirely to get results.

### A. Flight velocity

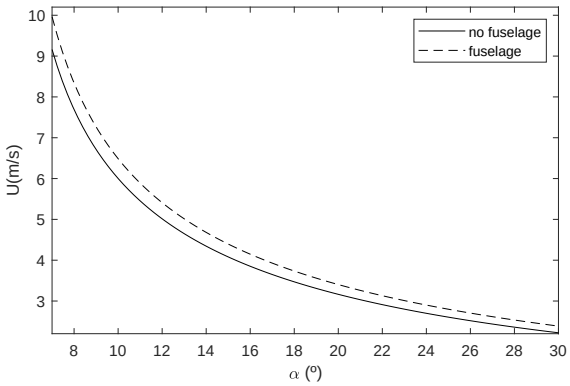


Fig. 12. Velocity as a function of the angle of attack

Ornithopters usually need low velocities in order to interact with the environment. Meanwhile, long distance flights may benefit from fast flights, due to energy savings. Therefore, the analysis of the velocity range, is useful to study the performance of the ornithopter, for both cases with and without the fuselage.

Using equations (3) and (8) we see in fig. 12 the velocity as a function of the angle of attack. As discussed above, the angle of attack is defined by the deflection of the tail with equation (8), and its relation does not change by adding the fuselage. Therefore, the lift coefficient of the wing and the tail remain the same. In addition, the lift coefficient of the body is almost negligible when compared to the contributions of wing and tail. Then, the main difference between both cases is due to the additional weight added by the fuselage.

The results show that, as expected, the ornithopter will fly faster with the fuselage. Therefore, for maneuvers at low speed, the fuselage is a disadvantage, as the minimum speed is bigger. On the other hand, for long flights, it would be interesting to study the flapping frequency needed to maintain flight, which should lead to a direct relation with the power consumption.

### B. Comparison with the angle of attack

Fig. 13 shows the thrust needed to fly at different angles of attack. These results are obtained using equation (9). We can see how the thrust grows at low angles of attack as the lift force generated by the wing is limited, needing a higher velocity which increases the drag. Note that the minimum thrust is obtained at a different point in both cases. This point corresponds to the minimum $C_D/C_L$ ratio, which changes due to the addition of the fuselage.

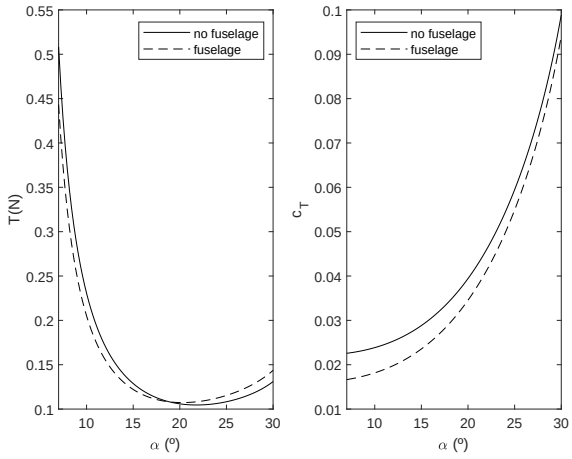


Fig. 13. Thrust and thrust coefficient needed as a function of angle of attack

The thrust coefficient provides a useful tool for the dimensional analysis and the influence of the weight. Hence, we see that the high thrust needed at low angles of attack is due to the high velocity. Then, when the angle of attack gets higher, the drag coefficient grows. However, this growth is noted at the dimensional thrust just at the highest angles of attack.

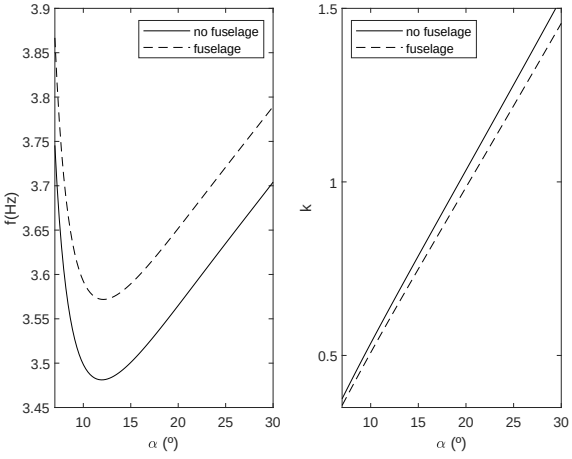


Fig. 14. Dimensional and reduced frequency as a function of angle of attack

Fig. 14 shows the flapping frequency for the studied range of the angle of attack. We see that the frequency needed is always higher for the prototype with the fuselage. Again, this is caused by the higher velocity that this vehicle has, as we see that the reduced frequency is very similar in both cases when plotted.

Note also the influence of the angle of attack on the formulation of the thrust. At high angles of attack, the difference in the thrust coefficient is lower, as seen in fig. 14. However, the difference in the reduced frequency needed is higher, caused by the cross terms with both variables ($\alpha$ and $k$).

To sum up, we have seen that, when the same angle of attack is considered, the frequency needed to fly with our fuselage is always bigger. However, the flight velocity with the fuselage is also higher, so a further comparison is needed to study those variables.

### C. Comparison with the flight velocity

Considering the velocity as the input variable, the analysis gets more practical. Now the power consumption concerns disappear, as the velocity gives the information about the distance traveled.

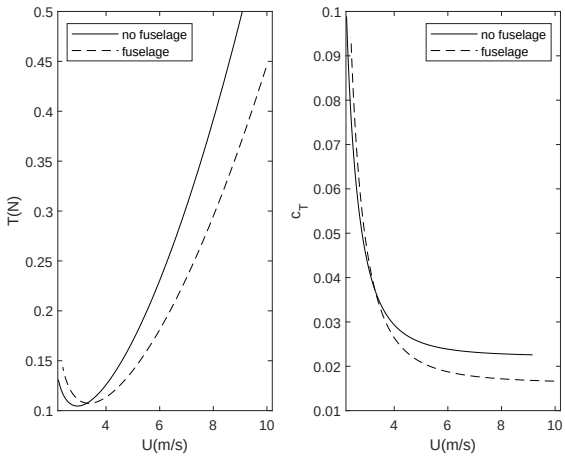


Fig. 15. Thrust and thrust coefficient needed as a function of the flight velocity

Fig. 15 shows an intersection between the two thrust curves. At low velocities, the weight of the fuselage causes the prototype to need more thrust. However, the reduction of drag becomes more significant as the velocity grows, and the fuselage provides an important advantage.

Note that, given the thrust as a function of the velocity, now the relation between both cases does not change for the dimensionless thrust coefficient. However, it is interesting to see how the thrust coefficient needed is almost constant from a certain velocity.

Note also that the minimum thrust is not obtained at the same velocity for both cases, as it was not at the same angle of attack neither. Then the velocity of minimum drag to lift ratio changes for both cases.

When the flapping frequency is considered as a function of the velocity (fig. 16), we see how when the velocity increases, the difference of frequency needed for both cases (with and without fuselage) gets lower. At high speeds, the fuselage provides an important aerodynamic advantage, as discussed before. Note that the dimensional frequency does not vary from a small range in all the operational conditions. In fact, it has a minimum at a certain flight condition which varies in both cases, as it depends on the aerodynamic characteristics of the ornithopter.

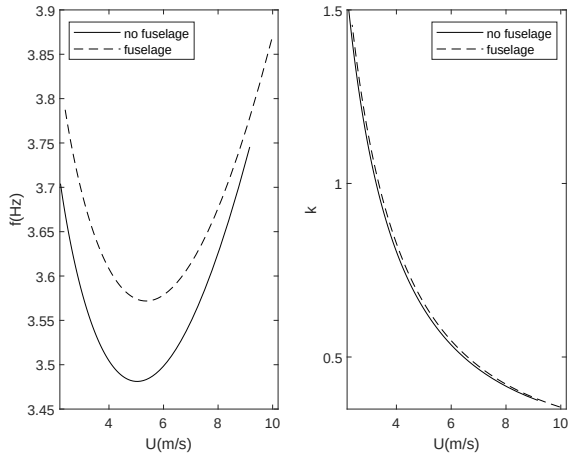


Fig. 16. Dimensional and reduced frequency as a function of the flight velocity

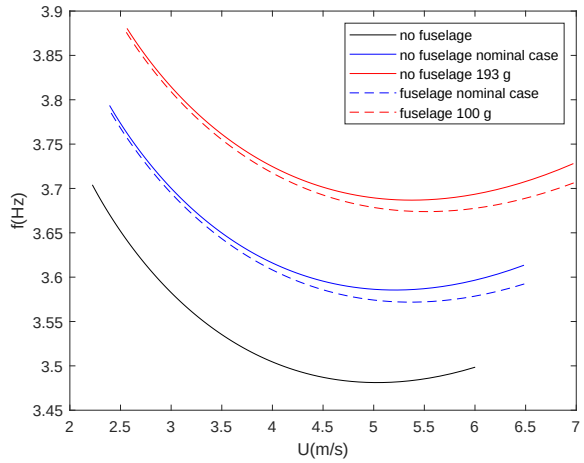


Fig. 17. Frequency vs flight velocity for different payloads

### D. Payload analysis

Fig. 17 shows a deeper analysis of the comparison between flight velocity and flapping frequency required. When we consider the same weight for the ornithopter, we see that, at low speeds, the aerodynamic performance of the fuselage adds no improvement to the flight performance. On the other hand, at high speeds, the fuselage gives better aerodynamic performance. Moreover, note that, with the same weight, the ornithopter is carrying 93 g more of payload.

## VI. Conclusions

The use of a suitable fuselage has not received significant attention in the research and development of small UAVs. However, the improved aerodynamics provided by the fuselage can compensate for the weight increase. In addition, the flight conditions of the ornithopter do not necessarily require a closed case to protect the on-board mechanisms, payload and electronics.

In this paper, we have studied the influence of the fuselage on the ornithopter flight. The aerodynamic forces have been obtained for the CFD analysis of the E-flap ornithopter, but the procedure can be generalized for any prototype.

The modification of the thrust coefficient due to the flexibility of the wings of an ornithopter is also a contribution of the paper.

Results obtained show how the added weight of the fuselage gives an operational disadvantage. The minimum velocity is directly related to the weight, so the ornithopter can fly slower without the fuselage, providing added maneuverability. In addition, the flapping frequency needed at a low velocity range is lower.

A general conclusion is the change on the optimal flight conditions when the fuselage is added, so the minimum thrust needed is found at different points of the operational range for both cases. In addition, the payload analysis shows that the fuselage provides advantages at high velocity. However, at low velocity flights, like those required for inspection, or immediately before perching, the added weight of the fuselage may not compensate for the aerodynamic advantage.

The benefit of the fuselage could be more evident in the hybrid fixed wing-flapping wing configuration developed in the AERIAL-CORE H2020 project [10]. In this case, substantial energy savings can be obtained in the reduction of the drag in the fixed wing flight mode, as the aerodynamics of the prototype change and the flight velocity gets higher.

## VII. Acknowledgment

The authors would like to thank to Lorena Calvente for her help with the fuselage design and Emanuela Savastano for her support on experimental data collection, as members of GRVC. The work of Javier Santaolaya and other members of the Center for Advanced Aerospace Technologies (CATEC) in the development and manufacturing of the fuselage is also acknowledged.

## References

[1] R. Malka, A. L. Desbiens, Y. Chen, and R. J. Wood, "Principles of microscale flexure hinge design for enhanced endurance," in *2014 IEEE/RSJ International Conference on Intelligent Robots and Systems*. IEEE, 2014, pp. 2879–2885.

[2] A. Ramezani, X. Shi, S.-J. Chung, and S. Hutchinson, "Bat bot (b2), a biologically inspired flying machine," in *2016 IEEE International Conference on Robotics and Automation (ICRA)*. IEEE, 2016, pp. 3219–3226.

[3] W. Yang, L. Wang, and B. Song, "Dove: A biomimetic flapping-wing micro air vehicle," *International Journal of Micro Air Vehicles*, vol. 10, no. 1, pp. 70–84, 2018.

[4] M. Hassanalian, A. Abdelkefi, M. Wei, and S. Ziaei-Rad, "A novel methodology for wing sizing of bio-inspired flapping wing micro air vehicles: theory and prototype," *Acta Mechanica*, vol. 228, no. 3, pp. 1097–1113, 2017.

[5] J. Gerdes, A. Holness, A. Perez-Rosado, L. Roberts, A. Greisinger, E. Barnett, J. Kempny, D. Lingam, C.-H. Yeh, H. A. Bruck, *et al.*, "Robo raven: a flapping-wing air vehicle with highly compliant and independently controlled wings," *Soft Robotics*, vol. 1, no. 4, pp. 275–288, 2014.

[6] G. A. Folkertsma, W. Straatman, N. Nijenhuis, C. H. Venner, and S. Stramigioli, "Robird: a robotic bird of prey," *IEEE robotics & automation magazine*, vol. 24, no. 3, pp. 22–29, 2017.

[7] R. Zufferey, J. Tormo-Barbero, M. M. Guzmán, F. J. Maldonado, E. Sanchez-Laulhe, P. Grau, M. Pérez, J. Á. Acosta, and A. Ollero, "Design of the high-payload flapping wing robot e-flap," *IEEE Robotics and Automation Letters*, vol. 6, no. 2, pp. 3097–3104, 2021.

[8] M. Guzmán, C. R. Páez, F. Maldonado, R. Zufferey, J. Tormo-Barbero, J. Á. Acosta, and A. Ollero, "Design and comparison of tails for bird-scale flapping-wing robots," in *2021 IEEE/RSJ International Conference on Intelligent Robots and Systems (IROS)*. IEEE, 2021, pp. 6358–6365.

[9] C. Ruiz, J. Á. Acosta, and A. Ollero, "Aerodynamic reduced-order volterra model of an ornithopter under high-amplitude flapping," *Aerospace Science and Technology*, p. 107331, 2022.

[10] . AERIAL CORE Grant 2019, "Action 871479," 2019, last accessed 18 February 2022. [Online]. Available: https://aerial-core.eu/

[11] "Fundación andaluza para el desarrollo aeroespacial y centro avanzado de tecnologías aeroespaciales, fada-catec." [Online]. Available: http://www.catec.aero/es

[12] R. Cano, C. Pérez, F. Pruaño, A. Ollero, and G. Heredia, "Diseño mecánico de un manipulador aéreo ligero de 6 gdl para la construcción de estructuras de barras," *ARCAS (ICT-2011–287617) del séptimo Programa Marco de la Comisión Europea y el proyecto CLEAR (DPI2011-28937-C02-01)*, 2013.

[13] M. Trujillo, A. Viguria, R. CANO, and A. OLLERO, "Sistema aéreo no tripulado con capacidad avanzada de manipulación," in *IV Congreso Nacional de I+D en Defensa y Seguridad (DESEi+d 2016)*.

[14] "Dianna project, applus, catec, airbus." [Online]. Available: https://blog.applus.com/dianna-development-of-new-technologies-for-the-automation-of-aeronautical-assembly-processes

[15] J. Alaminos-Quesada and R. Fernandez-Feria, "Propulsion of a foil undergoing a flapping undulatory motion from the impulse theory in the linear potential limit," *Journal of Fluid Mechanics*, vol. 883, 2020.